Advances in Differential Equations and Control Processes 2025, 32(3), 3050.
https://doi.org/10.59400/adecp3050

Article

Prescribed performance trajectory tracking control with dynamic adaptive sliding mode observer for quadrotor UAV

Qiu Xu*, Li Zhang

Yangzhou Polytechnic Institute, Yangzhou 225127, Jiangsu, China
*** Corresponding author:** Qiu Xu, xuqiu202507@126.com

CITATION

Xu Q, Zhang L. Prescribed performance trajectory tracking control with dynamic adaptive sliding mode observer for quadrotor UAV. Advances in Differential Equations and Control Processes. 2025; 32(3): 3050. https://doi.org/10.59400/adecp3050

ARTICLE INFO

Received: 2 April 2025
Revised: 19 May 2025
Accepted: 10 September 2025
Available online: 29 September 2025

Abstract: The trajectory tracking accuracy of quadrotor UAVs is greatly challenged by external disturbances and model uncertainties. To overcome these issues, this paper presents a prescribed performance control approach incorporating a dynamic adaptive sliding mode observer. First, external disturbances and model uncertainties are treated as lumped disturbances within the quadrotor UAV system. By designing a sliding mode observer with a nonlinear gain adjustment mechanism, these disturbances can be estimated and compensated for in real time, without requiring prior knowledge of their bounds. Building upon this, the prescribed performance function is further improved, and a new performance function independent of initial conditions is developed to find out that the system states converge within the predefined performance boundaries, achieving precise trajectory tracking. The system's convergence is rigorously analysed with Lyapunov stability theory. And we can make sure the method using lots of simulations. The results indicate algorithm achieves fast error convergence and precise trajectory tracking, even in the presence of dynamic environmental disturbances.

Keywords: UAV; prescribed performance control; adaptive sliding mode observer; disturbance estimation and compensation; nonlinear control strategy; finite-time convergence; aerial robotics

1. Introduction

During recent experiences, quadcopter UAVs have gradually demonstrated significant application potential in fields such as aerial photography, disaster detection, as well as intelligent logistics due to their unique characteristics such as vertical takeoff and landing, fixed-point hovering, and three-dimensional manoeuvring [1]. However, their underactuated and highly coupled nonlinear dynamics, coupled with external wind field disturbances, load mass changes, unmodeled dynamics, and other complex disturbances, pose a significant challenge to high-precision trajectory tracking control [2]. Therefore, the design of a robust and high-precision control strategy to achieve stable trajectory tracking of a quadrotor UAV in a complex and disturbed environment has become a hot research topic [3].

In control strategy research, traditional control methods such as PID [4] and LQR [5] are widely used for algorithmic structure. Then we can find that it is not difficult to implement. However, these methods, which are based on linearised models, generally suffer from reduced control accuracy and insufficient robustness in the face of model uncertainties and external disturbances [6]. Although subsequent research has proposed improved schemes such as fractional-order PID control [7] and adaptive PID control [8] which have improved the robustness of the system to some extent, the control effect in complex nonlinear scenarios is still limited. Furthermore, with the

rapid development of Micro-Electro-Mechanical Systems technology, it provides key technical support for the miniaturization and high-performance development of small quadrotor UAVs.

To handle the shortcomings about conventional control methods, significant research efforts have been devoted to advanced nonlinear control techniques, including adaptive control [9] and sliding mode control [10]. In Ref. [11] investigates a fixed-time tracking control scheme for nonlinear systems by integrating funnel control methodology with a dynamic event-triggered strategy. In Ref. [12] proposes an adaptive robust control framework to address the trajectory tracking challenge for UAV operating under uncertain conditions, demonstrating substantial improvement in closed-loop robustness. In Ref. [13], disturbance compensation is achieved by extending the state observer, and effective trajectory tracking is achieved in a two-dimensional plane but is not extended to a three-dimensional environment. In Ref. [14], the adaptive control optimized by the genetic algorithm improves the efficiency of parameter tuning, but it is difficult to ensure real-time control performance under complex disturbances. Sliding mode control has consistently attracted interest in flight control applications owing to its remarkable resilience against model uncertainties and external perturbations [15]. The integral adaptive sliding mode controller designed in [16] significantly improves the system stability by improving the disturbance rejection. The fast terminal sliding mode control law developed in [17] effectively improves convergence rate with actuator failure by improving the asymptotic law. However, the existing sliding mode control method generally suffers from high-frequency chatter, and the accuracy of the estimation of compound disturbances still needs to be improved.

Many existing observer designs rely on the premise that the disturbance derivative remains bounded [18], a condition that is often challenging to satisfy in real-world applications. To address this issue, an adaptive neural network observer incorporating an online learning mechanism was proposed in [19], which effectively estimates nonuniform and time-varying disturbances. Furthermore, a fixed-time sliding mode observer introduced in [20] offers a novel approach by eliminating the dependence on initial conditions when estimating disturbances. Nonetheless, it is important to emphasize that the majority of current observer frameworks still depend on the boundedness assumption of disturbance derivatives, limiting their practicality in engineering scenarios.

Building on recent developments in the field, this work introduces a control framework that integrates a sliding mode observer with an enhanced prescribed performance approach to address the problem of precise trajectory tracking for quadrotor UAVs under some disturbances. The framework first employs a sliding mode observer to dynamically evaluate and counteract aggregated disturbances. Next, a novel control law is formulated under the prescribed performance paradigm, ensuring that the system trajectories consistently conform to a predefined performance bound. The overall stability about resulting closed-loop system is rigorously proven with strict Lyapunov-based analysis. Numerical experiments are used to determine the approach. The key study can be outlined:

a) Develop a sliding mode observer capable of finite-time estimation of compound disturbances without requiring prior knowledge of disturbance bounds.

b) A prescribed performance sliding mode controller is proposed. Unlike traditional prescribed performance control, the proposed method not only achieves asymmetric error constraints but is also no longer constrained by initial values.

2. Model description and problem formulation

In this work, a cascaded control architecture is adopted, partitioning the trajectory tracking task into two interrelated subsystems: the outer-loop position controller and the inner-loop attitude controller. This hierarchical arrangement facilitates targeted optimization at each layer, thereby improving the overall system performance.

Two reference coordinate systems are introduced to model the quadrotor UAV's spatial behavior: an inertial frame $(O_E X_E Y_E Z_E)$ and a body-fixed frame $(O_B X_B Y_B Z_B)$. The inertial frame, which follows the right-hand rule, is anchored to the ground, while the origin of the body coordinate system is located at the UAV's center of mass, with its axes aligned with the UAV's physical structure. The geometric relationship between these two frames is illustrated in **Figure 1**.

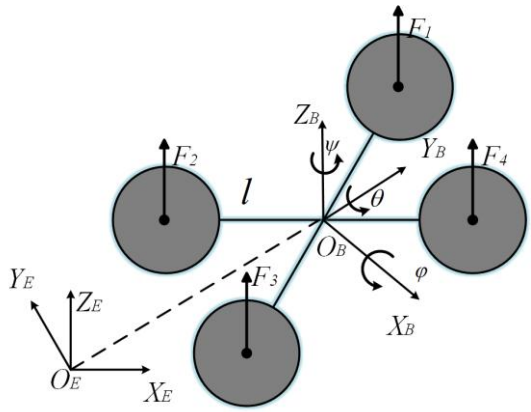

Figure 1. Coordinate system relationship diagram.

In **Figure 1**, φ, θ, ψ represents the three attitude angles.

The transformation between the inertial and body coordinate frames is realized through a sequence of three rotational operations. The resulting coordinate transformation matrix $\boldsymbol{R}$, which captures the orientation of the UAV in space, is presented in Equation (1),

$$\boldsymbol{R} = \begin{bmatrix} \mathrm{c}(\theta)\mathrm{c}(\psi) & \mathrm{s}\varphi\mathrm{c}(\psi)\mathrm{s}(\theta) - \mathrm{c}\varphi\mathrm{s}(\psi) & \mathrm{s}(\theta)\mathrm{c}(\psi)\mathrm{c}(\varphi) + \mathrm{s}(\varphi)\mathrm{s}(\psi) \\ \mathrm{c}(\theta)\mathrm{s}(\psi) & \mathrm{s}\varphi\mathrm{s}(\psi)\mathrm{s}(\theta) - \mathrm{c}\varphi\mathrm{c}(\psi) & \mathrm{s}(\theta)\mathrm{s}(\psi)\mathrm{c}(\varphi) - \mathrm{s}(\varphi)\mathrm{c}(\psi) \\ -\mathrm{s}(\theta) & \mathrm{c}(\theta)\mathrm{s}(\varphi) & \mathrm{c}(\theta)\mathrm{c}(\varphi) \end{bmatrix} \tag{1}$$

where $\mathrm{c}(\bullet)$ and $\mathrm{s}(\bullet)$ are the functions $\cos(\bullet)$ and $\sin(\bullet)$ respectively.

This transformation matrix not only establishes the conversion relationship between position coordinates but also provides the mathematical basis for modeling attitude kinematics. The four input variables for torque control of the four-rotor motors of a quadcopter are:

$$\begin{cases} u_A = F_A + F_B + F_C + F_D \\ u_B = (F_A + F_D - F_B - F_C)l/\sqrt{2} \\ u_C = (F_A + F_B - F_C - F_D)l/\sqrt{2} \\ u_D = (F_D + F_B - F_A - F_C)l \end{cases} \tag{2}$$

where l is the distance from the motor to the quadcopter's center of gravity， and $F_{A,}F_B, F_C, F_D$ is the lift generated by the four motors of the quadcopter.

With the Newton-Euler equations, the dynamic model of a quadcopter can be decomposed into positional motion and attitude motion. Considering the symmetry of the geometric structure and assuming that the Euler angles of the quadcopter are bounded, i.e. $-\pi/2 < \varphi < \pi/2$, $-\pi/2 < \theta < \pi/2$ and $-\pi < \psi < \pi$ [21]. The system dynamics can be mathematically described as:

$$\begin{cases} \ddot{x} = \dfrac{1}{m}[u_A(c(\varphi)s(\theta)c(\psi) + c(\varphi)c(\psi))] - \dfrac{K_x}{m}\dot{x} + \dfrac{d_x}{m} \\ \ddot{y} = \dfrac{1}{m}[u_A(\mathrm{c}(\varphi)\mathrm{s}(\theta)\mathrm{s}(\psi) - \mathrm{s}(\varphi)\mathrm{c}(\psi))] - \dfrac{K_y}{m}\dot{y} + \dfrac{d_y}{m} \\ \ddot{z} = \dfrac{1}{m}[u_A(\mathrm{c}(\varphi)\mathrm{c}(\theta) - mg)] - \dfrac{K_z}{m}\dot{z} + \dfrac{d_z}{m} \\ \ddot{\varphi} = \dfrac{1}{I_x}[u_B + (I_y - I_z)\dot{\theta}\dot{\psi} - K_\varphi\omega_\varphi + d_\varphi] \\ \ddot{\theta} = \dfrac{1}{I_y}[u_C + (I_z - I_x)\dot{\varphi}\dot{\psi} - K_\theta\omega_\theta + d_\theta]] \\ \ddot{\psi} = \dfrac{1}{I_z}[u_D + (I_x - I_y)\dot{\varphi}\dot{\theta} - K_\psi\omega_\psi + d_\psi]] \end{cases} \tag{3}$$

where $i = x, y, z$ denotes the position, $\ddot{i}$ shows the linear acceleration, and I_i is the moment of inertia about each principal axis. g corresponds to gravitational acceleration, while $\ddot{\varphi}, \ddot{\theta}, \ddot{\psi}$ indicates the angular acceleration associated with the UAV's attitude. $d_l (l = x, y, z, \varphi, \theta, \psi)$ accounts for external disturbances affecting both position and attitude, and m denotes the mass of the quadrotor.

3. Sliding mode controller design

The presented control strategy integrates a dynamic adaptive sliding mode observer with a prescribed performance control mechanism to achieve accurate trajectory tracking. As illustrated in **Figure 2**, the control architecture primarily consists of a dynamic adaptive sliding mode observer and a prescribed performance function controller, ultimately achieving high-precision trajectory tracking control. d_i and d_j represent externally applied dynamic disturbances to the system, where $i = (x, y, z), j = (\varphi, \theta, \psi)$ ， f_i and f_j denote the actual disturbances acting on the system, while $\hat{f}_i$ and $\hat{f}_j$ correspond to the disturbance estimates. obtained from the observer. ξ_i the position transformation error.

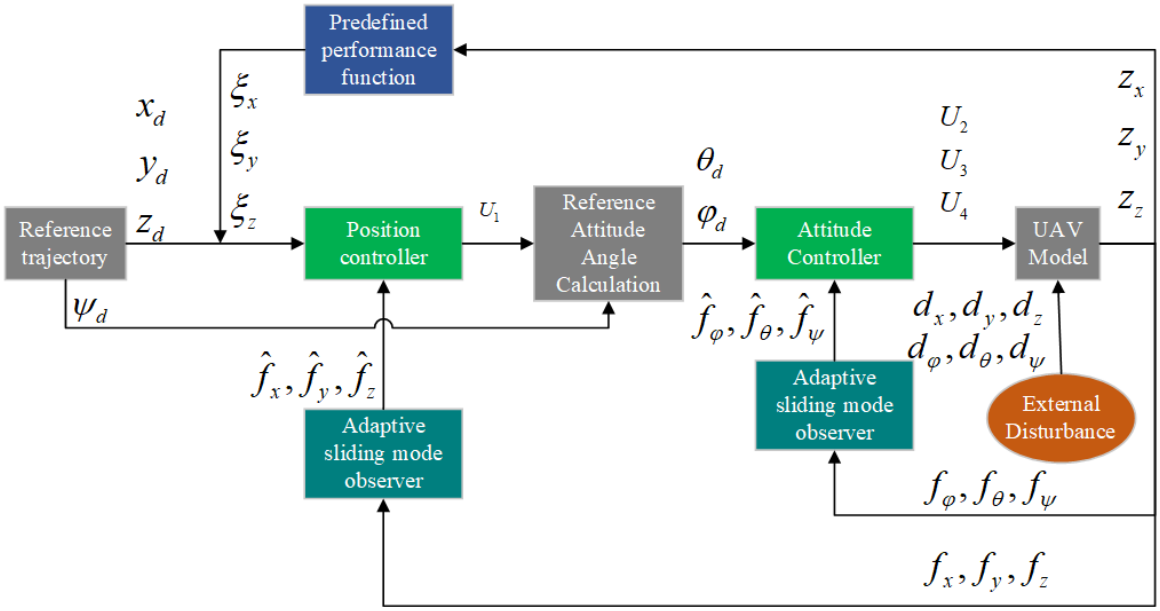

Figure 2. Control system block diagram.

3.1. Design of a finite-time sliding mode observer

The proposed sliding mode observer is designed without the assumption that the derivative of the disturbance is zero, nor does it require the disturbance to satisfy the precondition of boundedness. The specific design process is as follows.

Equation (3) can be reformulated as:

$$\vartheta_l = u_l + f_l, l = x, y, z, \varphi, \theta, \psi \tag{4}$$

where are $\vartheta_x = \dot{x}$, $\vartheta_y = \dot{y}$, $\vartheta_z = \dot{z}$, $\vartheta_\varphi = \dot{\varphi}$, $\vartheta_\theta = \dot{\theta}$ $\vartheta_\psi = \dot{\psi}$, $u_\varphi = U_2 I_x^{-1}$, $u_\theta = U_3 I_y^{-1}$, $u_\psi = U_4 I_z^{-1} f_x = d_x m^{-1} - K_x{}^{m^{-1}} \dot{x}$, $f_y = d_y m^{-1} - K_y m^{-1} \dot{y}$, $f_z = d_z m^{-1} - K_z m^{-1} \dot{z} f_\varphi = d_\varphi I_x^{-1} - K_\varphi \omega_\varphi I_x^{-1}$, $f_\theta = d_\theta I_y^{-1} - K_\theta \omega_\theta I_y^{-1}$, $f_\psi = d_\psi I_z^{-1} - K_\psi \omega_\psi I_z^{-1}$.

Design assistance error is:

$$e_l = \varpi_l - \vartheta_l \tag{5}$$

where the auxiliary variable is defined as:

$$\dot{\varpi}_l = u_l + \omega_l - \lambda_l e_l - \lambda_l e_l^\eta \tag{6}$$

Of these, λ_l, λ_l and η are positive definite parameters, η satisfies $0 < \eta < 1$, and ω_l is an intermediate control variable.

The formulation of the non-singular fast terminal sliding mode surface is given by:

$$\chi_l = \dot{e}_l + \lambda_l e_l + \lambda_l e_l^\eta \tag{7}$$

There is a relationship as follows:

$$\begin{aligned}\chi_l &= \dot{e}_l + \hat{\lambda}_l e_l + \lambda_l e_l^{\eta} \\ &= \dot{\varpi}_l - \dot{\vartheta}_l + \hat{\lambda}_l e_l + \lambda_l e_l^{\eta} \\ &= u_l + \omega_l - \hat{\lambda}_l e_l - \lambda_l e_l^{\eta} - u_l - f_l + \hat{\lambda}_l e_l + \lambda_l e_l^{\eta} \\ &= \omega_l - f_l\end{aligned} \tag{8}$$

Differentiating Equation (8) yields:

$$\dot{\chi}_l = \dot{\omega}_l - \dot{f}_l \tag{9}$$

Lemma 1 [22] Consider the following system:

$$\dot{z} = -m_1 z - m_2 z^{q_2} \tag{10}$$

where z is the system state and $m_1 \in \mathbb{R}_+$, $m_2 \in \mathbb{R}_+$, $0 < q_2 < 1$. If these conditions are satisfied, the system exhibits global fast finite-time stability, with the upper bound of the settling time T is:

$$T \le \frac{1}{m_1(1-q_2)} \ln\left(\frac{m_1 z_0^{1-q_2} + m_2}{m_2}\right) \tag{11}$$

Combined with Lemma 1, the design is:

$$\dot{\omega}_l = -(\gamma_l + \delta_l)\tanh(\chi_l) \tag{12}$$

γ_l represents a positive definite constant, and the control gain δ_l is defined as:

$$\begin{cases} \dot{\delta}_l = -(A_l + a_l)\tanh(\sigma_l) \\ \dot{a}_l = \begin{cases} b_l|\sigma_l|, |\sigma_l| > \Delta_l \\ 0, \quad |\sigma_l| \le \Delta_l \end{cases} \end{cases} \tag{13}$$

where A_l, Δ_l and b_l are positive definite parameters and the variables σ_l and $\bar{u}_l$ are defined as:

$$\begin{cases} \sigma_l = \delta_l - \dfrac{1}{\alpha_{l,1}}|\bar{u}_l| - \varepsilon_l \\ \dot{\bar{u}}_l = -\dfrac{1}{\alpha_{l,2}}\left[(\gamma_l + \delta_l)\tanh(\chi_l) + \bar{u}_l\right] \end{cases} \tag{14}$$

where ε_l, $\alpha_{l,1}$ and $\alpha_{l,2}$ are positive definite parameters.

Lemma 2 [23] considers the dynamic equations of the system:

$$\dot{\sigma}(t) = a(t) + u_s(t) \tag{15}$$

where the sliding mode variable serves as the control input, while the uncertainty satisfies condition $|\dot{a}(t)| < a_1$. The control input is defined as follows:

$$u_s(t) = -(k_s(t) + \eta_s)\mathrm{sgn}(\sigma(t)) \tag{16}$$

where $k_s(t)$ and η_s are rational numbers.

The adaptive law is:

$$\begin{cases} \dot{k}_s(t) = -\left[R_s + r_s(t)\right]\mathrm{sgn}(\delta_s) \\ \dot{r}_s(t) = \begin{cases} \gamma_s \mid \delta_s(t) \mid, & \text{if } \mid \delta_s(t) \mid > \Delta_s \\ 0, & \text{otherwise} \end{cases} \end{cases} \tag{17}$$

Than:

$$\begin{cases} \delta_s(t) = k_s(t) - \dfrac{1}{a_s} \le \left|\bar{u}_s\right| - \dot{o}_s \\ \dot{\bar{u}} = \dfrac{1}{\tau_s}(-\bar{u}_s + u_s) \end{cases} \tag{18}$$

There are parameters $a_s < 1$, $\dot{o}_s$, Δ_s and γ_s that meet the conditions.

$$\frac{1}{4}\dot{o}_s^2 > \Delta_s^2 + \frac{1}{\gamma_s}\left(\frac{q_s a_1}{\alpha_s}\right)^2 \tag{19}$$

where q_s is called the safety margin and the system implements sliding mode motion for a limited finite time.

According to Lemma 2, $\delta_l > \dot{f}_l$ can be satisfied in a limited time. At the same time, the sliding mode surface χ_l is stable for a finite time T_χ. Then, $\dot{e}_l + \dot{\lambda}_l e_l + \lambda_l e_l^\eta = 0$. Combining Lemma 1, the error e_l is stable in a finite time T_e. The disturbances can then be observed through $\hat{f}_l = \omega_l = f_l$, and the observer has a stable time satisfying $T_1 = T_e + T_\chi$.

3.2. Design about finite-time position sliding mode controller

Finite-time sliding mode control strategy is put forward to reach accurate position tracking. Given coupled dynamics about the position system, it is decomposed into two subsystems: horizontal motion and altitude control. To ensure precise trajectory tracking, the UAV's three-dimensional position tracking error is defined as follows:

$$z_i = i - i_d \tag{20}$$

where $z_i (i = x, y, z)$ represents the position tracking errors along three axes, i_d denotes the desired position inputs, and i is the actual position output. By differentiating both sides of Equation (20), we obtain:

$$\dot{z}_i = \dot{i} - \dot{i}_d \tag{21}$$

where $\dot{z}_i$, $\dot{i}_d$ and $\dot{i}$ are the derivatives of z_i, i_d and i respectively.

The design prescribes a prescribed performance function of:

$$\begin{cases} \alpha(t) = (\alpha_0 - \alpha_\infty)\exp(-\zeta t) + \alpha_\infty \\ \beta(t) = (\beta_0 - \beta_\infty)\exp(-\zeta t) + \beta_\infty \end{cases} \tag{22}$$

where α_0 、 β_0 and α_∞ 、 β_∞ represent the initial and terminal values of the prescribed performance function, respectively, and ζ is positive-definite design parameter.

Define a finite-time function:

$$\rho_i = z_i(0)\exp\left(1-\frac{\bar{T}}{\bar{T}-t}\right),(i=x,y,z) \tag{23}$$

where $\bar{T}$ is a time parameter, the error satisfies:

$$-\alpha_i(t) < z_i < \beta_i(t) \tag{24}$$

where $z_i = z_{i0} - \rho_i$.

Different from the traditional prescribed performance function, the proposed one has two distinct features: first, it does not require the upper and lower boundaries to be symmetric; second, it is no longer constrained by the initial value.

To achieve the prescribed performance constraints, the transfer function is designed as:

$$\Gamma_i(\xi_i) = \frac{\beta_i \exp\left(\xi_i + \ln\left(\alpha_i/\beta_i\right)\right) - \alpha_i}{\exp\left(\xi_i + \ln\left(\alpha_i/\beta_i\right)\right) + 1} \tag{25}$$

Differentiating with respect to it yields:

$$\begin{aligned}\dot{\xi}_i &= \frac{\dot{\alpha}_i + \dot{z}_i}{\alpha_i + z_i} - \frac{\dot{\beta}_i - \dot{z}_i}{\beta_i - z_i} - \frac{\dot{\alpha}_i}{\alpha_i} + \frac{\dot{\beta}_i}{\beta_i} \\ &= \left(\frac{1}{\alpha_i + z_i} + \frac{1}{\beta_i - z_i}\right)\dot{z}_i + \frac{\dot{\alpha}_i}{\alpha_i + z_i} - \frac{\dot{\beta}_i}{\beta_i - z_i} - \frac{\dot{\alpha}_i}{\alpha_i} + \frac{\dot{\beta}_i}{\beta_i} \\ &= \ell_i \dot{z}_i + \pi_i\end{aligned} \tag{26}$$

where $\ell_i = \left(\frac{1}{\alpha_i + z_i} + \frac{1}{\beta_i - z_i}\right), \pi_i = \frac{\dot{\alpha}_i}{\alpha_i + z_i} - \frac{\dot{\beta}_i}{\beta_i - z_i} - \frac{\dot{\alpha}_i}{\alpha_i} + \frac{\dot{\beta}_i}{\beta_i}$, taking a second derivative yields:

$$\ddot{\xi}_i = \ell_i \ddot{z}_i + \dot{\ell}_i \dot{z}_i + \dot{\pi}_i \tag{27}$$

The position control system utilizes a non-singular fast terminal sliding surface, defined as follows:

$$s_i = \dot{\xi}_i + p_i \xi_i + q_i \xi_i^{\iota} \tag{28}$$

where p_i, q_i, and ι are the control coefficients of the sliding mode surface and ι satisfies $0 < \iota < 1$.

Differentiating both sides give:

$$\begin{aligned}\dot{s}_i &= \ddot{\xi}_i + p_i \dot{\xi}_i + \iota q_i \dot{\xi}_i \xi_i^{\iota-1} \\ &= \ell_i \ddot{z}_i + \dot{\ell}_i \dot{z}_i + \dot{\pi}_i + \left(\ell_i \dot{z}_i + \pi_i\right)\left(p_i + \iota q_i \xi_i^{\iota-1}\right)\end{aligned} \tag{29}$$

The control strategy for the position subsystem is expressed as:

$$u_i = \left(-k_{1i}s_i - k_{2i}s_i^{2\iota-1} - \dot{\ell}_i\dot{z}_i - \dot{\pi}_i - \left(\ell_i\dot{z}_i + \pi_i\right)\left(p_i + \iota q_i\xi_i^{\iota-1}\right)\right)\ell_i^{-1} - \hat{d}_i + \ddot{\rho}_i + \ddot{\imath}_d \tag{30}$$

where k_{1i} and k_{2i} are positive definite parameters.

3.3. Finite time attitude controller design

To achieve an accurate attitude tracking target, the three-dimensional attitude tracking error of the UAV is defined as:

$$z_j = j - j_d \tag{31}$$

where $j_d(j = \varphi, \theta, \psi)$ denotes the desired attitude input, and j represents the actual measured attitude angle. By differentiating both sides, we obtain:

$$\dot{z}_j = \dot{j} - \dot{j}_d \tag{32}$$

where $\dot{z}_j$, $\dot{j}_d$ 和 $\dot{j}$ are the derivatives of z_j, z_j and j respectively.

The attitude control system adopts the following non-singular fast terminal sliding mode:

$$s_j = \dot{z}_j + p_i z_j + q_i z_j^{\iota} \tag{33}$$

where p_j and q_j are the control coefficients.

Differentiating both sides gives:

$$\dot{s}_j = \ddot{z}_j + p_j\dot{z}_j + q_j\iota z_j^{\iota-1}\dot{z}_j \tag{34}$$

The attitude control law is designed as:

$$u_j = I_i\left(-k_{1j}s_j - k_{2j}s_j^{2\iota-1} - p_j\dot{z}_j - q_j\iota z_j^{\iota-1}\dot{z}_j - \hat{d}_j + \ddot{j}_d\right) \tag{35}$$

3.4. Convergence analysis

Construct a Lyapunov function:

$$V_c = \sum_{l=x,y,z,\varphi,\theta,\psi} \frac{1}{2}s_l^2 \tag{36}$$

Its derivative is given by:

$$\dot{V}_c = \sum_{l=x,y,z,\varphi,\theta,\psi} -k_{1l}s_l^2 - k_{2l}s_l^{2\iota} = \sum_{l=x,y,z,\varphi,\theta,\psi} -k_1V_c - k_2V_c^{\iota} \tag{37}$$

where $k_1 = 2k_{1l}, k_2 = 2^{\iota}k_{2l}^{\iota}$.

Lemma 1 shows that the sliding mode surface is stable for finite time.

Given the established sliding surface, the following can be derived:

$$\begin{cases} \dot{\xi}_i + p_i\xi_i + q_i\xi_i^{\iota} = 0 \\ \dot{z}_j + p_jz_j + q_jz_j^{\iota} = 0 \end{cases} \tag{38}$$

Lemma 1 shows that ξ_i and z_j are stable for finite time T_z.

According to finite-time function theory, ρ_i vanishes in $\bar{T}$ time units, leading to the conclusion that the control system settles at the origin in finite time $T = \max\{\bar{T}, T_1 + T_s + T_z\}$. Combining this with the definition of prescribed power, one can demonstrate that the condition $\alpha_i(t) - \rho_i < z_i < \rho_i + \beta_i(t)$ is consistently upheld.

4. Simulation results and analysis

To make sure efficacy and superior performance of the proposed dynamic adaptive sliding mode observer-based prescribed performance control strategy, comprehensive numerical simulations are conducted using a nonlinear dynamic model of a quadrotor UAV. The MATLAB/Simulink environment is employed as the simulation platform for implementing the control algorithms and assessing their performance. For comparative analysis, we select the adaptive terminal sliding mode control approach developed in [24] as the comparative method.

The numerical simulation experiment parameters are set as follows: the given reference trajectory is described as a cylindrical spiral curve with $i_d = [\cos(t), \sin(t) + 1, 5 + t]^T$, the given reference yaw angle is $\psi = \pi/6$, and the given initial state is $[i_0, j_0]^T = [0.5, 0.5, 4.5, 0, 0, 0]^T$. The observer parameters are λ_l=10, λ_l=10, η=0.5, γ_l=10, $\alpha_{l,1}$=1, $\alpha_{l,2} = 2$, $\varepsilon_l = 1$, $\Delta_l = 1$.The model parameters and controller parameters of the quadrotor UAV are given in **Tables 1** and **2** respectively.

Set the dynamic external disturbance to be:

$$d_l = 0.5\sin(0.01t) + 0.5\sin(l) \tag{39}$$

Table 1. Parameters about the quadrotor UAV model.

Parameter/Unit	**Numerical value**
m/kg	2
g/(m.s²)	9.8
L/m	0.30
I_x	1.24
I_y	1.24
I_z	2.50

Table 2. Parameters about controller.

Parameter/Unit	**Numerical value**
p_i, p_j	2,5
q_i, q_j	6,7,8,2,2,2
$k_{1i,} k_{1j}$	20,35
$k_{2i,} k_{2j}$	15,20

Figures 3–5 depict the comparative position tracking errors along the x-, y-, and z-axes, with the prescribed performance boundaries delineated by solid black lines (upper limit) and dashed black lines (lower limit). The blue dashed line corresponds to the comparative method from previous literature. In terms of dynamic performance, the settling time of the proposed method in the x-direction (0.6 s) is significantly shorter than that of the conventional method (1 s), and this improvement in response speed directly demonstrates the advantage of the proposed strategy in dynamic tracking processes. Within the 1–4 s interval with disturbance effects, the error curve of the comparative method exhibits significant oscillations, whereas the error convergence of the proposed method is more stable, indicating that it can more effectively suppress the impact of disturbances on tracking accuracy in anti-interference scenarios, thereby maintaining the smoothness of the convergence process.

Details in the magnified subplot reveal that although the overshoot of the proposed strategy is slightly larger than that of the comparative method, the fluctuations during error convergence are gentler with more regular amplitude variations, avoiding the high-frequency, irregular oscillations observed in the comparative method. This demonstrates the characteristic of the proposed control strategy in balancing convergence speed and stability.

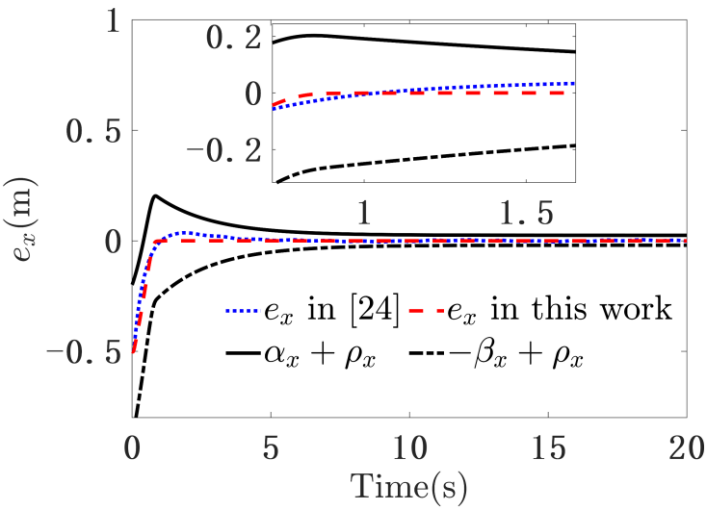

Figure 3. x Trajectory tracking error.

In terms of steady-state accuracy, the z-direction comparison shows that the error of the comparative method still exhibits noticeable fluctuations in the steady state, while the error of the proposed strategy can be maintained more stably within a smaller range. This difference stems from the effective error constraint of the proposed method — through the design of prescribed performance boundaries, the error is consistently confined within the predefined range, reducing disturbance interference in the steady state and thus achieving higher tracking accuracy. Overall, the error curve of the proposed control strategy never exceeds the prescribed performance boundaries throughout the process, and its convergence smoothness is significantly superior to that of the comparative method, which fully validates the role of prescribed performance boundaries in ensuring the accuracy and stability of error convergence.

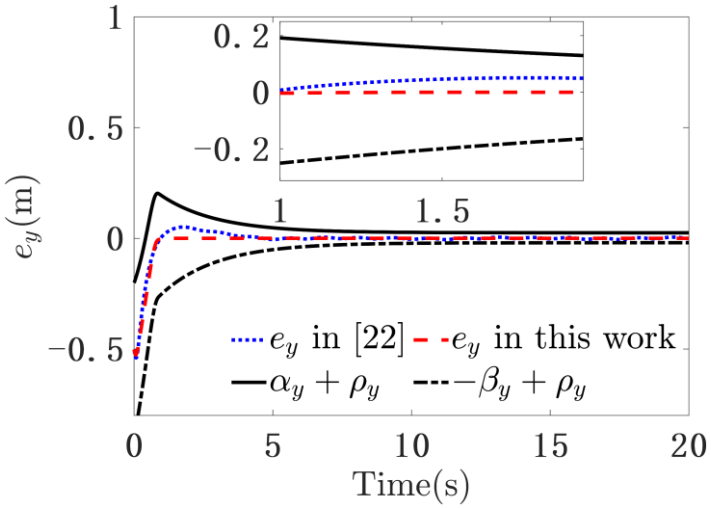

Figure 4. y Trajectory tracking error.

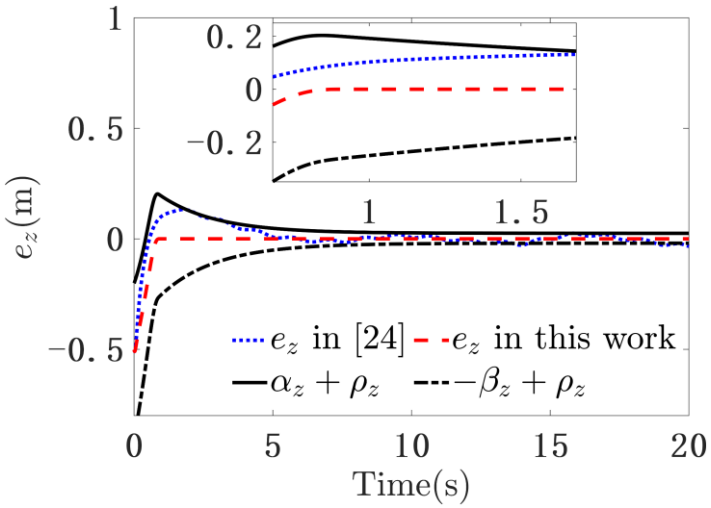

Figure 5. z Trajectory tracking error.

Figure 6 further indicates that the proposed control strategy exhibits superior tracking performance in the complex trajectory segment of ascending spiral, particularly at critical points with varying trajectory curvature, where the error control is more precise, reflecting its strong tracking capability under dynamically complex trajectories.

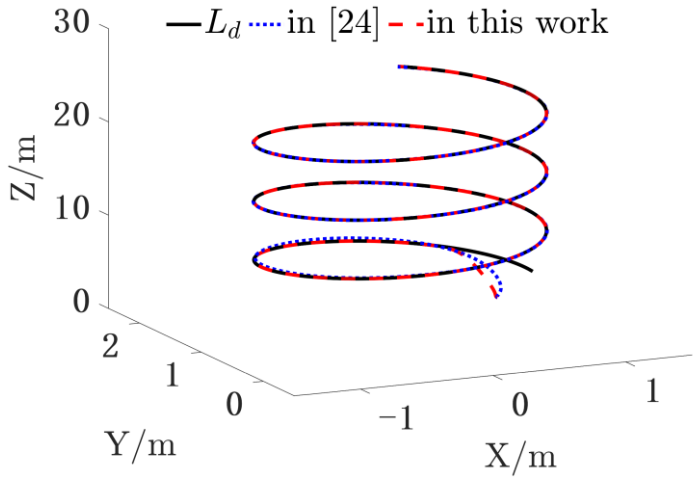

Figure 6. Trajectory tracking effect.

The attitude error responses are illustrated in **Figures 7–9**. It is evident from the results that the proposed strategy facilitates rapid and steady error convergence across all attitude angles. In contrast, the comparative method exhibits slower convergence, along with unstable error fluctuations during the transient phase, suggesting suboptimal flight attitude control. By comparison, the proposed strategy ensures consistently stable attitude regulation throughout the flight.

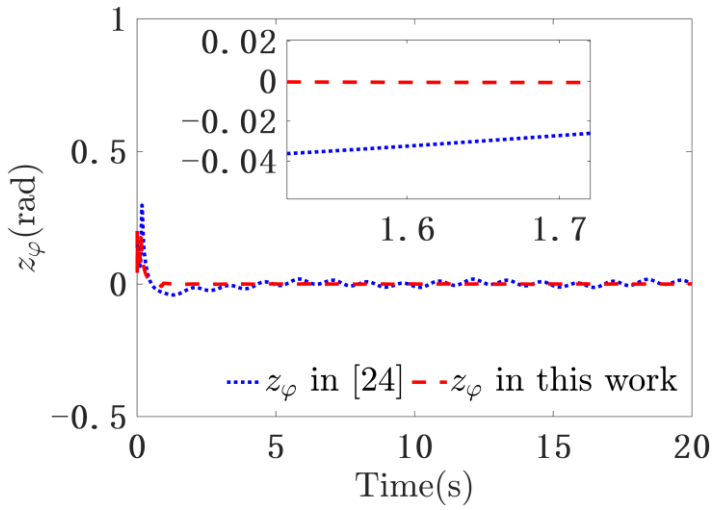

Figure 7. φ tracking error.

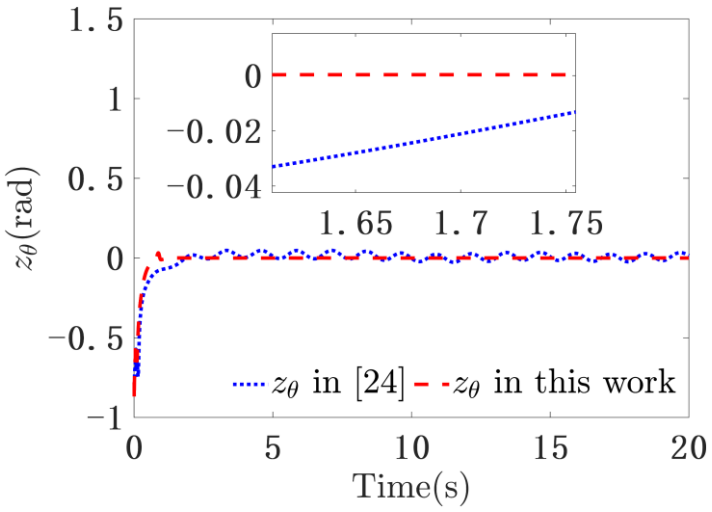

Figure 8. θ tracking error.

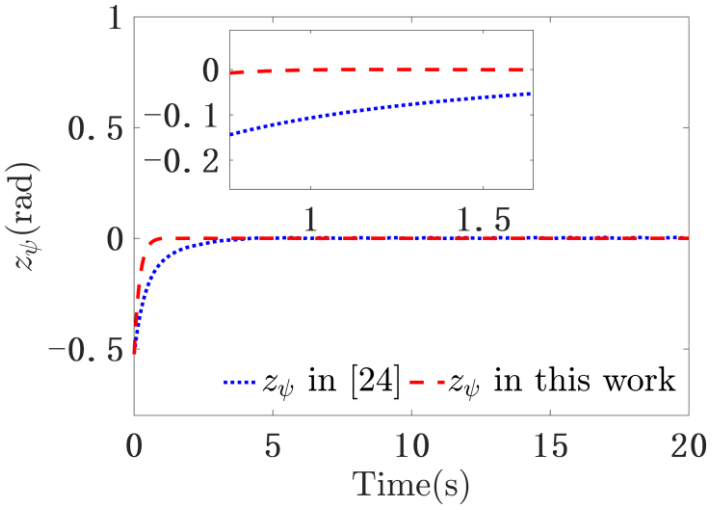

Figure 9. ψ tracking error.

The disturbance estimation performance of the proposed observer is presented in **Figures 10** and **11** for position and attitude angle, respectively. As shown, the actual system disturbance (red dashed line) and the observer's estimated disturbance (blue solid line) demonstrate close agreement. The results indicate that the observer achieves rapid and accurate estimation of both position and attitude disturbances, regardless of disturbance variations. These findings confirm the observer's excellent disturbance estimation capability.

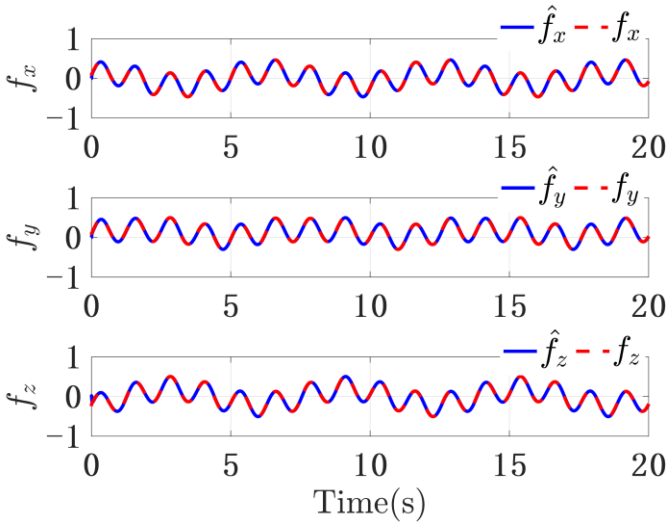

Figure 10. Position disturbance observation

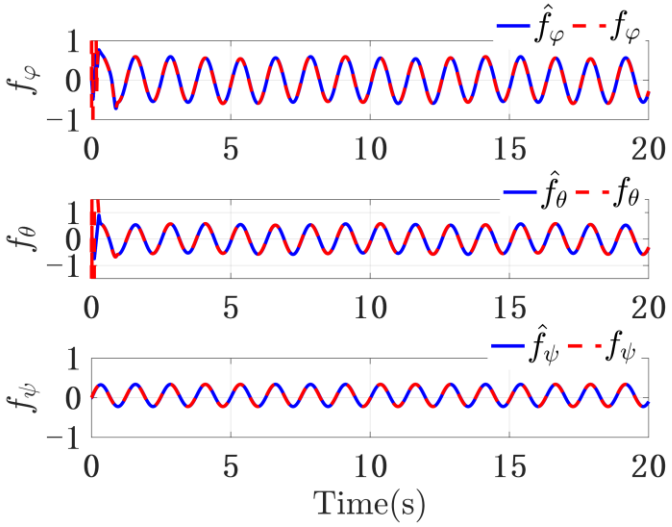

Figure 11. Attitude disturbance observation.

5. Conclusion

This paper proposes an advanced prescribed performance control scheme that integrates a dynamic adaptive sliding mode observer to achieve precise trajectory tracking about quadrotor UAVs in the presence about model uncertainties and external disturbances. The key contributions are summarized as follows:

a) A newly developed sliding mode observer featuring exponential convergence properties, where finite-time convergence of disturbance estimation errors is rigorously guaranteed through an advanced dynamic adaptive law;

b) An innovative prescribed performance function formulation that effectively regulates the system error dynamics.

Extensive simulation studies demonstrate the proposed method's enhanced robustness and superior tracking performance under various disturbance scenarios, achieving a significant improvement in trajectory tracking accuracy. Future work will first focus on the problem of optimal control allocation under input saturation constraints, and further improve control accuracy and robustness through algorithm

optimization. Secondly, it will deepen the research on multi-UAV cooperative control, and improve the theoretical modeling and simulation verification of formation coordination and anti-disturbance strategies. Finally, it will promote the construction of physical quadrotor platforms and conduct real-flight verification to bridge the gap between numerical simulation and practical application.

Author contributions: Qiu Xu: Writing - original draft, Conceptualization, Software. Li Zhang: Writing - review & editing, Conceptualization, Funding acquisition, Methodology.

Funding: This research was supported by the Doctoral Special Project of Jiangsu Province's "Double Creation Program" (2408014/003) and the topic Design and Research on Perceptual User Selection Based on Scoring Region Subspace (223202).

Conflict of interest: There is no conflict of interes.

References

1. Liang H, Li J, Zhang Y. Adaptive super-twisted sliding mode trajectory tracking control for quadrotor UAV with prescribed performance based on finite-time disturbance observer. Engineering Research Express. 2024; 6(3): 035551. doi: 10.1088/2631-8695/ad70f3
2. Hawashin D, Nemer M, Gebreab SA, et al. Blockchain applications in UAV industry: Review, opportunities, and challenges. J Journal of Network and Computer Applications. 2024; 230: 103932. doi: 10.1016/j.jnca.2024.103932
3. Li S, Yang X, Wang X, et al. Learning target-aware vision transformers for real-time UAV tracking. IEEE Transactions on Geoscience and Remote Sensing. 2024; 62: 1-15. doi: 10.1109/TGRS.2024.3417400
4. Lopez-Sanchez I, Moreno-Valenzuela J. PID control of quadrotor UAVs: A survey [J]. Annual Reviews in Control, 2023, 56: 100900.
5. Dhewa OA, Arifin F, Priyambodo AS, et al. Attitude UAV Stability Control Using Linear Quadratic Regulator-Neural Network (LQR-NN). IIUM Engineering Journal. 2024; 25(2): 246-265. doi: 10.31436/iiumej.v25i2.3119
6. Javed S, Hassan A, Ahmad R, et al. State-of-the-art and future research challenges in UAV swarms. IEEE Internet of Things Journal. 2024; 11(11): 19023-19045. doi: 10.1109/JIOT.2024.3364230
7. Delgado-Reyes G, Valdez-Martínez JS, Guevara-López P, et al. Hover Flight Improvement of a Quadrotor Unmanned Aerial Vehicle Using PID Controllers with an Integral Effect Based on the Riemann–Liouville Fractional-Order Operator: A Deterministic Approach. Fractal and Fractional. 2024; 8(11): 634. doi: 10.3390/fractalfract8110634
8. Sahrir NH, Basri MAM. Intelligent PID Controller Based on Neural Network for AI-Driven Control Quadcopter UAV. International Journal of Robotics and Control Systems. 2024;4(2):691-708.
9. Liu P, Tian H, Wang H. Research on Control of Quadrotor UAV Based on Improved BP Neural Network PID and ADRC. In: Proceedings of the 2024 IEEE 2nd International Conference on Sensors, Electronics and Computer Engineering (ICSECE); 29–31 August 2024; Jinzhou, China. pp. 104-112. doi: 10.1109/ICSECE61994.2024.10671617
10. Baek J, Kang M. A synthesized sliding-mode control for attitude trajectory tracking of quadrotor UAV systems. IEEE/ASME Transactions on Mechatronics. 2023; 28(4): 2189-2199. doi: 10.1109/TMECH.2022.3230755
11. Wang Y, Zong G. Dynamic event-triggered adaptive fixed-time practical tracking control for nonlinear systems through funnel function. IEEE Transactions on Automation Science and Engineering. 2025; 7008-7017. doi: 10.1109/TASE.2024.3458176
12. Chen G, Wang W, Dong J. Performance-Optimize Adaptive Robust Tracking Control for USV-UAV Heterogeneous Systems with Uncertainty. IEEE Transactions on Vehicular Technology. 2025; 74(5): 7251-7262. doi: 10.1109/TVT.2025.3526360
13. Bie G, Chen X. UAV trajectory tracking based on ADRC control algorithm. ITM Web of Conferences. 2022; 47: 02017. doi: 10.1051/itmconf/20224702017
14. Shui J, Peng D. Application research on improved genetic algorithm and active disturbance rejection control on quadcopters. Measurement and Control. 2024; 57(9): 1347-1357. doi: 10.1177/00202940241240408
15. Zheng EH, Xiong JJ, Luo JL. Second order sliding mode control for a quadrotor UAV. ISA transactions. 2014; 53(4): 1350-1356.

16. Eltayeb A, Rahmat MF, Basri MAM, et al. Integral adaptive sliding mode control for quadcopter UAV under variable payload and disturbance. IEEE Access. 2022; 10:94754-94764. doi: 10.1109/ACCESS.2022.3203058
17. Gao B, Liu YJ, Liu L. Adaptive neural fault-tolerant control of a quadrotor UAV via fast terminal sliding mode. Aerospace Science and Technology. 2022; 129: 107818. doi: 10.1016/j.ast.2022.107818
18. Kim HH, Lee MC, Kyung JH, Do HM. Evaluation of force estimation method based on sliding disturbances observer for dual-arm robot system. International Journal of Control, Automation and Systems. 2021; 19(1): 1-10. doi: 10.1007/s12555-019-0324-x
19. Liu K, Yang P, Wang R, et al. Observer-based adaptive fuzzy finite-time attitude control for quadrotor UAVs. IEEE Transactions on Aerospace and Electronic Systems. 2023; 59(6): 8637-8654. doi: 10.1109/TAES.2023.3308552
20. Li B, Gong W, Yang Y, et al. Appointed fixed time observer-based sliding mode control for a quadrotor UAV under external disturbances. IEEE Transactions on Aerospace and Electronic Systems. 2022; 58(1): 290-303. doi: 10.1109/TAES.2021.3101562
21. Laghari AA, Jumani AK, Laghari RA, Nawaz H. Unmanned aerial vehicles: A review. Cognitive Robotics. 2023; 3: 8-22. doi: 10.1016/j.cogr.2022.12.004
22. Wu C, Hui J, Yan J, et al. Dynamic modeling and faster finite-time attitude stabilization of receiver aircraft for aerial refueling. Nonlinear Dynamics. 2021; 104: 467-481. doi: 10.1007/s11071-021-06288-4
23. Li H, Lin X. Robust fault-tolerant control for dynamic positioning of ships with prescribed performance. Ocean Engineering. 2024; 298: 117314. doi: 10.1016/j.oceaneng.2024.117314
24. Mofid O, Mobayen S, Zhang C, Balasubramanian E. Desired tracking of delayed quadrotor UAV under model uncertainty and wind disturbance using adaptive super-twisting terminal sliding mode control. ISA transactions. 2022; 123: 455-471. doi: 10.1016/j.isatra.2021.06.002